Cellular/Molecular

$\alpha_2\delta3$ Is Essential for Normal Structure and Function of Auditory Nerve Synapses and Is a Novel Candidate for Auditory Processing Disorders

Antonella Pirone,[1]* Simone Kurt,[2,3]* Annalisa Zuccotti,[1] Lukas Rüttiger,[1] Peter Pilz,[4] David H. Brown,[5] Christoph Franz,[1] Michaela Schweizer,[6] Marco B. Rust,[7] Rudolf Rübsamen,[5] Eckhard Friauf,[8] Marlies Knipper,[1] and Jutta Engel[9,10]

[1]University of Tübingen, Department of Otolaryngology, Tübingen Hearing Research Centre, Molecular Physiology of Hearing, 72076 Tübingen, Germany, [2]Cluster of Excellence "Hearing4all," Institute of Audioneurotechnology and Hannover Medical School, Department of Experimental Otology, ENT Clinics, 30625 Hannover, Germany, [3]University of Ulm, Institute of Neurobiology, 89081 Ulm, Germany, [4]University of Tübingen, Institute of Neurobiology, 72076 Tübingen, Germany, [5]University of Leipzig, Institute of Biology II, 04103 Leipzig, Germany, [6]University of Hamburg, Center for Molecular Neurobiology, 20251 Hamburg, Germany, [7]University of Kaiserslautern, Department of Biology, Neurobiology/Neurophysiology Group, 67653 Kaiserslautern, Germany, [8]University of Kaiserslautern, Department of Biology, Animal Physiology Group, 67653 Kaiserslautern, Germany, [9]University of Tübingen, Department of Physiology II and Tübingen Hearing Research Centre, 72076 Tübingen, Germany, and [10]Saarland University, Department of Biophysics, 66421 Homburg/Saar, Germany

The auxiliary subunit $\alpha_2\delta3$ modulates the expression and function of voltage-gated calcium channels. Here we show that $\alpha_2\delta3$ mRNA is expressed in spiral ganglion neurons and auditory brainstem nuclei and that the protein is required for normal acoustic responses. Genetic deletion of $\alpha_2\delta3$ led to impaired auditory processing, with reduced acoustic startle and distorted auditory brainstem responses. $\alpha_2\delta3^{-/-}$ mice learned to discriminate pure tones, but they failed to discriminate temporally structured amplitude-modulated tones. Light and electron microscopy analyses revealed reduced levels of presynaptic Ca^{2+} channels and smaller auditory nerve fiber terminals contacting cochlear nucleus bushy cells. Juxtacellular *in vivo* recordings of sound-evoked activity in $\alpha_2\delta3^{-/-}$ mice demonstrated impaired transmission at these synapses. Together, our results identify a novel role for the $\alpha_2\delta3$ auxiliary subunit in the structure and function of specific synapses in the mammalian auditory pathway and in auditory processing disorders.

Key words: **auditory discrimination learning; Ca^{2+} channel; CACNA2D3; endbulb of Held; inner hair cell; spiral ganglion**

Introduction

Voltage-gated calcium channels (VGCCs) are protein complexes composed of a main, pore-forming α_1 subunit and auxiliary $\alpha_2\delta$ and β subunits. The traditional view is that auxiliary subunits modulate biophysical properties of VGCCs, which are mostly determined by the α_1 subunit, and assist in trafficking and proper surface expression of the channel complex (Catterall, 2000; Dolphin, 2012). Recent evidence, however, suggests an additional role of $\alpha_2\delta$ subunits in synaptogenesis (Eroglu et al., 2009; Kurshan et al., 2009; Dolphin, 2012). $\alpha_2\delta$ subunits, encoded by one of the four genes *CACNA2D1-CACNA2D4*, consist of a large extracellular glycosylated α_2 peptide linked to a small membrane-anchored δ peptide (Davies et al., 2007; Dolphin, 2012). Coexpression of the isoforms $\alpha_2\delta1$–3 with various α_1 and β subunits results in functional channels with increased current amplitudes and altered channel gating (Arikkath and Campbell, 2003).

Rat brain analysis has revealed specific, partially overlapping expression patterns for $\alpha_2\delta1$–3 mRNA, with $\alpha_2\delta3$ being particularly expressed in some auditory regions (Cole et al., 2005). Analysis of $\alpha_2\delta$ mutant mice has demonstrated distinct, cell-specific functions for each $\alpha_2\delta$ isoform. Cardiomyocytes of $\alpha_2\delta1$ knockout-mice show decreased Ca^{2+} currents with altered kinetics (Fuller-Bicer et al., 2009). Ducky mice with mutated, nonfunctional $\alpha_2\delta2$ display cerebellar dysfunction, indicating that a lack of $\alpha_2\delta2$ in $Ca_v2.1/\beta4$ complexes in cerebellar Purkinje cells cannot be compensated by other $\alpha_2\delta$ isoforms (Barclay et al., 2001; Donato et al., 2006). The mammalian *CACNA2D3*, encoding for

Received July 20, 2013; revised Nov. 8, 2013; accepted Nov. 21, 2013.

Author contributions: A.P., S.K., L.R., P.P., C.F., M.S., R.R., E.F., M.K., and J.E. designed research; A.P., S.K., A.Z., L.R., P.P., D.H.B., C.F., M.S., M.B.R., R.R., E.F., M.K., and J.E. performed research; S.K. contributed unpublished reagents/analytic tools; A.P., S.K., A.Z., L.R., P.P., D.H.B., C.F., M.S., M.B.R., R.R., E.F., M.K., and J.E. analyzed data; A.P., S.K., A.Z., L.R., P.P., D.H.B., C.F., M.S., M.B.R., R.R., E.F., M.K., and J.E. wrote the paper.

This work was supported by EU-CAVNET MRTN-CT-2006-035367, RIMB (University of Kaiserslautern), DFG SFB 894, and PP1608 (Saarland University). Experiments were performed at the Hearing Research Centre and the Institute of Neurobiology at the University of Tübingen, the Institute of Neurobiology at the University of Ulm, the Institute of Biology II at the University of Leipzig, the Center for Molecular Neurobiology at the University of Hamburg, the Department of Biology at the University of Kaiserslautern, and the Department of Biophysics at Saarland University. We thank S. Kasperek, K. Rohbock, J. Ihl, T. Kehrwald, and C. Raithore for excellent technical assistance; Drs. M. Müller and S. Münkner for help with data analysis; and Dr. M. Jacob for helpful discussion.

The authors declare no competing financial interests.

*A.P. and S.K. contributed equally to this work.

Correspondence should be addressed to Dr. Prof. Jutta Engel, Department of Biophysics (Building 76), Saarland University, 66421 Homburg/Saar, Germany. E-mail: jutta.engel@mx.uni-saarland.de.

A. Pirone's present address: Tufts Medical School, Department of Neuroscience, Boston, Massachusetts 02115.

D.H. Brown's present address: Program in Neuroscience, Department of Psychology, Florida State University, Tallahassee, Florida 32306.

DOI:10.1523/JNEUROSCI.3085-13.2014

 0270-6474/14/340434-12$15.00/0

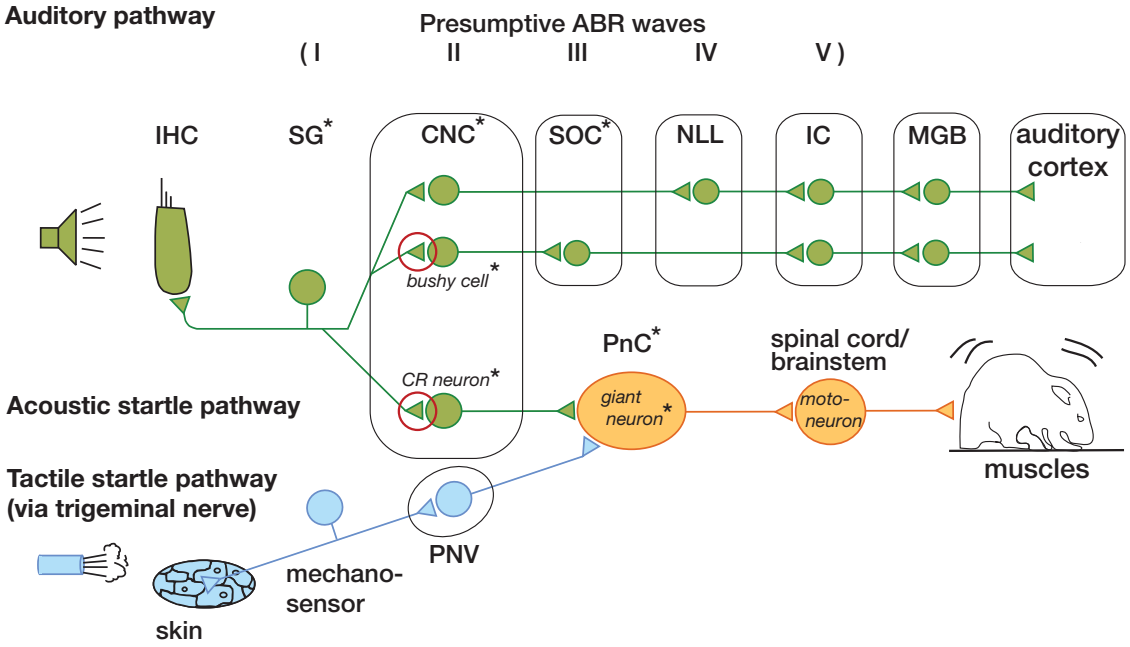

Figure 1. Basic scheme of the primary auditory pathway, the primary acoustic startle pathway, and the trigeminal tactile startle pathway, and expression of $\alpha_2\delta3$. Elements of the primary auditory pathway are depicted in the upper part. Spiral ganglion (SG) neurons give rise to auditory nerve fibers and project to neurons of the cochlear nuclear complex (CNC), such as bushy cells (BCs) in the ventral CN. BCs in turn project predominantly into the superior olivary complex (SOC). Information is further transmitted into the inferior colliculus (IC). Some CNC neurons project into the nuclei of the lateral lemniscus (NLL) and the IC. After being processed in the medial geniculate body (MGB), ascending auditory information is finally represented in the auditory cortex. In mice, ABR waves I–V appear to reflect information processing in the cochlea (wave I), the CNC (wave II), the SOC (wave III), the NLL (wave IV), and the IC (wave V). Middle row, The primary acoustic startle pathway shares IHCs and SG neurons with the primary auditory pathway. Auditory nerve fibers form synapses on cochlear root (CR) neurons, specialized neurons located in the auditory nerve. These CR neurons project to giant neurons in the caudal pontine reticular formation (PnC), which themselves contact motoneurons innervating facial or body muscles. Bottom row, The trigeminal tactile startle pathway includes pseudo-unipolar mechanosensory neurons in the skin, which activate neurons in the principal nucleus V (PNV), which in turn project onto PnC giant neurons. Bouton-like auditory nerve fiber terminals on BCs or CR neurons (red circles) were smaller in $\alpha_2\delta3^{-/-}$ mice. *:$\alpha_2\delta3$ expression in neurons of the respective relay station (see Results). Modified from Simons-Weidenmaier et al. (2006), with permission.

$\alpha_2\delta3$, and the *Drosophila* ortholog *stj* have been identified as pain genes. Mice and fruit flies lacking *CACNA2D3* and *stj*, respectively, show impaired avoidance of noxious heat (Neely et al., 2010), which in mice was attributed to impaired transmission of thermal pain-evoked signals from thalamus to higher pain centers (Neely et al., 2010).

Here, we have studied the role of $\alpha_2\delta3$ on VGCCs and signal transmission specifically along the auditory pathway. Auditory brainstem responses (ABRs) and sophisticated behavioral tasks were used to explore hearing function of $\alpha_2\delta3$-knock-out mice ($\alpha_2\delta3^{-/-}$), which show an impaired acoustic startle response (SR; http://jaxmice.jax.org/strain/005780.html). The primary auditory pathway and the acoustic startle pathway share peripheral structures up to auditory nerve fiber (ANF) terminals (compare Fig. 1). We analyzed the effects of $\alpha_2\delta3$ gene deletion at various levels of the auditory system, from Ba^{2+} currents in inner hair cells (IHCs) to *in vivo* juxtacellular recordings at ANF–bushy cell (BC) synapses, to morphological analyses. Our findings demonstrate that $\alpha_2\delta3$ deletion alters the morphology and impairs the function of ANF synapses to their target neurons, resulting in impaired processing in the auditory and the acoustic startle pathway and in striking auditory discrimination deficits.

Materials and Methods

Animals. Mice with a targeted deletion of the *CACNA2D3* gene coding for $\alpha_2\delta3$ with insertion of a bacterial β-galactosidase under its promoter (B6.129P2-Cacna2d3^{tm1Dgen}) were generated by Deltagen (Neely et al., 2010) and purchased through The Jackson Laboratory. If not stated otherwise, cochleae and brains were dissected after mice had been killed by decapitation without (up to postnatal day 9 [P9]) or after anesthesia with CO_2 (older than P15). Animals were housed with free access to food and water at an average temperature of 22°C and a 12 h light-dark cycle. All experiments were carried out in accordance with the European Communities Council Directive (86/609/EEC) and approved by regional board for scientific animal experiments in Tübingen and Leipzig, Germany.

Acoustic and tactile SR measurements. Acoustic SR and prepulse inhibition (PPI) were measured as previously described (Plappert et al., 2006). Acoustic SR was measured as peak-to-peak vertical force in a time window of 50 ms beginning at the startle stimulus onset, minus spontaneous motor activity measured as peak-to-peak force in a time window of 50 ms before stimulation. Acoustic startle stimuli were 20 ms white noise bursts with an intertrial interval of 15 s. The background noise inside the sound-absorbing chambers was 32 dB root-mean-square in the acoustic experiments. Prepulses were 20 ms noise stimuli, 35–65 dB in 10 dB steps given 50 ms before startle stimuli over a background noise of 32 dB. Two startle stimulus sound pressure levels (SPLs) were used in the PPI experiment, 85 and 105 dB. PPI was only evaluated in mice with startle amplitudes >10 mN and is given as percentage decrease of startle amplitude. Thresholds of acoustic startle were measured as described previously (Pilz and Schnitzler, 1996). Startle threshold was determined in mice whose input–output function was about linear in the range of 75–105 dB SPL (26 of 33 mice). The suprathreshold parts of these individual functions were linearly extrapolated to threshold = 0 N. Tactile SRs using 90 Pa air puffs were recorded as described previously (Pilz et al., 2004). The sound of the air puff was masked by a 93 dB root-mean-square background noise. After mice were adapted to the setup, 8 stimuli with 105 dB were given for habituation in the acoustic startle experiments. Thereafter, each stimulus SPL was given 16 times in pseudorandom order to each mouse. In the PPI experiments (Fig. 2*B*), the mice first received 12 habituation startle stimuli (105 dB), which were not evaluated. Then they received each prepulse condition 20 times and each startle-stimulus-alone condition 30 times each. For the tactile startle experiment (Fig. 2*C*),

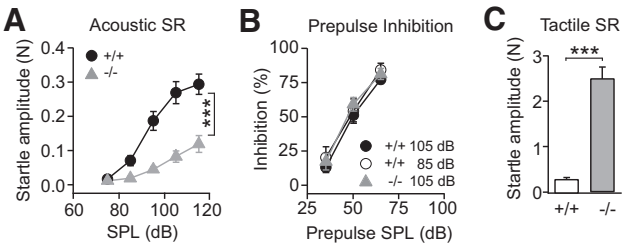

Figure 2. Acoustic and tactile SRs. ***A***, Amplitudes of the acoustic SR increased with increasing SPL of the stimulus. $\alpha_2\delta3^{+/+}$ mice ($n = 17$) had higher startle amplitudes than $\alpha_2\delta3^{-/-}$ mice ($n = 16$; general linear model, effect of genotype). ***$p < 0.001$. ***B***, Prepulse inhibition was very similar in $\alpha_2\delta3^{+/+}$ and $\alpha_2\delta3^{-/-}$ mice ($n = 17$, $n = 15$). Prepulses of 35–65 dB SPL were given before the acoustic startle stimulus of 105 dB SPL. For comparison, such prepulses were also given to $\alpha_2\delta3^{+/+}$ mice before a startle stimulus of 85 dB SPL ($n = 16$; open circles). ***C***, Amplitude of the tactile SR was on average 7.9-fold higher in $\alpha_2\delta3^{-/-}$ than in $\alpha_2\delta3^{+/+}$ mice ($n = 16$, $n = 17$). ***$p < 0.001$ (*t* test). ***A–C***, Error bars indicate mean ± SEM.

100 tactile stimuli were given with an intertrial interval of 15 s. Each condition was first averaged for each individual mouse; then means and statistical tests were calculated from these averages. A general linear model was calculated with startle stimulus SPL as continuous factor and genotype as the second factor. A 2-factor ANOVA was calculated with prepulse SPL as one factor and genotype as the other factor.

Hearing measurements. ABR and cubic $2 \times f1 - f2$ distortion product otoacoustic emissions (DPOAEs) for the two stimulus primaries (with frequency f1 and f2 and sound pressure level L1 and L2 for the first and the second primary, respectively) with $f2 = 1.24 \times f1$ and $L2 = L1 - 10$ dB were recorded in anesthetized mice aged 4 weeks as described previously (Engel et al., 2006; Rüttiger et al., 2013). For anesthesia, a mixture of ketamine-hydrochloride (75 mg/kg body weight, Ketavet 100, Pharmacia) and xylazine-hydrochloride (5 mg/kg body weight, Rompun 290, Bayer) was injected intraperitoneally with an injection volume of 5 ml/kg body weight. Anesthesia was maintained by subcutaneous application of one-fourth to one-third of the initial dose, typically in 20–30 min intervals. Body temperature was maintained by a temperature-controlled heating pad. ABR thresholds were determined with click (100 μs) or pure tone stimuli (2–45 kHz) with electrodes placed at the ear (positive) and vertex (reference). Outer hair cell (OHC) function was assessed by the maximum of the DP-gram and growth function of DPOAE.

RT-PCR, riboprobe synthesis, and in situ hybridization. RNA from mouse cochlea, brain, and IHCs was isolated and cDNA synthesis was performed as described previously (Baig et al., 2011). A 356 bp fragment specific for $\alpha_2\delta3$ was amplified using the primers 5′-TACATTGACAGC ACCCTCCC-3′ and 5′- GCATTTCGTAACACATCATCCC-3′ (Accession No. NM_009785). For RT-PCR of pooled IHCs, nested PCR was performed using nested primers 5′-CACAGATGTCCCAGTTAAAG AG-3′ and 5′-ACTTCAGAGAGATCCACACTAC-3′, yielding a 183 bp fragment. The PCR product was sequenced to confirm $\alpha_2\delta3$ specificity. Using the same primers, riboprobes were synthesized and *in situ* hybridization was carried out according to Singer et al. (2008). Analyses were performed in triplicates.

LacZ-staining. β-Galactosidase activity was detected and analyzed in $\alpha_2\delta3^{-/-}$ mice using the reporter function of the *CACNA2D3* construct. Cochleae were fixed and stained as described previously (Winter et al., 2009). Staining of 30-μm-thick brainstem sections was performed in staining solution containing 0.1% X-Gal (Hentschke et al., 2009). Photomicrographs were obtained with an Axioskop2 microscope (Zeiss) equipped with a CCD camera (F-View, Olympus; or DP-20, Olympus) using cell-F 3.0 software (Olympus) for analysis.

Immunohistochemistry. Cochleae of 4- to 5-week-old mice were isolated and prepared as described previously (Knirsch et al., 2007; Zampini et al., 2010). Alternatively, mice were deeply anesthetized and perfused transcardially with 4% paraformaldehyde, 15% picric acid in 100 mM PBS. Cochleae were dissected and postfixed for 30 min, whereas brains were postfixed overnight. Sections were stained with antibodies against $Ca_v2.1$ (SynapticSystems), VGLUT1 (SynapticSystems), $Ca_v1.3$ (Alomone Labs), or CtPB2/RIBEYE (BD Transduction Laboratories). Primary antibodies were detected with Cy3-conjugated (Jackson ImmunoResearch Laboratories) or Alexa-488/Alexa-568-conjugated secondary antibodies (Invitrogen). Immunolabeling was analyzed in at least three specimens of ≧3 animals using an Olympus BX61 microscope equipped with epifluorescence illumination. Images were acquired using a CCD camera and analyzed with cellSens software (Olympus Soft Imaging Solutions). For IHC immunolabeling, image stacks were acquired with complete coverage of the IHC nucleus (*z*-stack) and 3-dimensionally deconvoluted (Zampini et al., 2010). Figures 5*G*,*H*, 6, and 7*A–D* show projection images of all layers of a *z*-stack. For analysis of anti-$Ca_v2.1$ labeling of spiral ganglion (SG), neurons were imaged over a distance of 6 μm in a *z*-stack consisting of 20 layers and 3-dimensionally deconvoluted using cellSens ADVMLE deconvolution algorithm (Olympus Soft Imaging Solutions) to reach confocal-like resolution. Statistical analysis was performed on maximum intensity projection images using Fiji, an extension of ImageJ (Schindelin et al., 2012). The background was subtracted from the channel of interest (red), and a thresholded binary image was created. $Ca_v2.1$-positive puncta were counted if they extended over at least 4 pixels^2 (pixel size = 68.5 nm) or 0.019 μm^2. Puncta were counted automatically in a selected region. Their number was normalized to the number of SG somata and statistically analyzed using the Wilcoxon rank test. For analysis of VGLUT1-positive boutons (Fig. 7*A–D*), conventional images focused on the maximum perimeter of a neuron were processed with ImageJ software (http://rsbweb.nih.gov/ij/). The channel of interest was subjected to background subtraction, and a thresholded binary image was created. Area and perimeters of boutons of a selected area were analyzed automatically. Bouton sizes were statistically analyzed using the Wilcoxon rank test.

Electron microscopy and measurements of endbulbs of Held. Three $\alpha_2\delta3^{-/-}$ and $\alpha_2\delta3^{+/+}$ mice from three litters 4–5 weeks of age were prepared as described previously (Lappe-Siefke et al., 2009). For immunolabeling, 100 μm vibratome sections cut at the coronal plane and containing the ventral cochlear nucleus (VCN) were incubated with 10% horse serum containing 0.2% BSA (blocker) for 15 min to block nonspecific binding sites, and then incubated with guinea pig anti-VGLUT1 (SynapticSystems; 1:1000) in PBS containing 1% horse serum and 0.2% BSA (Carrier) overnight. The sections were washed with PBS, then incubated with biotinylated goat anti-guinea pig IgG (Vector Laboratories) diluted 1:1000 in Carrier for 90 min. After rinsing, they were incubated with ABC (Vector Labs) diluted 1:100 in PBS for 90 min. The sections were washed in PBS and reacted in diaminobenzidine-H_2O_2 solution (Sigma) for 10 min. Sections were either mounted on glass coverslips for light microscopic observation or postfixed with 1% osmium tetroxide (w/v), dehydrated, and further polymerized in Epon. Semithin sections (0.5 μm) from the VCN were cut, regions with VGLUT1-positive terminals onto BCs were selected, and ultrathin sections (60 nm) were collected, stained with uranyl acetate and lead citrate on pioloform-coated grids, and examined with a Zeiss EM 902. Pictures of VGLUT1-positive terminals contacting BCs with at least one obvious postsynaptic density were taken with a digital camera (MegaView III; Olympus) at a magnification of 12,000×. Bouton areas were measured and analyzed with ITEM software (Olympus).

Electrophysiological recordings. Acutely dissected organs of Corti of the apical turn were used to record Ba^{2+} currents (I_{Ba}) through Ca^{2+} channels (Knirsch et al., 2007). The bath solution contained the following (in mM): 72 lactobionate●NaOH, 40 NaCl, 35 TEA, 15 4-AP, 10 $BaCl_2$, 10 HEPES, 5.6 KCl, 5.6 glucose, 1 $MgCl_2$, pH 7.35, 320 mosmol/kg; the pipette solution (in mM) as follows: 110 Cs^+ methane sulfonate, 20 CsCl, 10 Na^+ phosphocreatine, 5 HEPES, 5 EGTA, 4 $MgCl_2$, 4 Na_2ATP, 0.3 GTP, 0.1 $CaCl_2$, pH 7.35, 305 mosmol/kg. Uncompensated series resistance was corrected by 80%. Linear leak subtraction was done off-line, and voltages were corrected by subtracting a liquid junction potential of 8.1 mV. I–V curves were fitted to a second-order Boltzmann function times driving force to determine parameters of the I_{Ba} activation curve, the voltage of half-maximum activation, V_h, and the slope factor, k, according to the following equation:

$$I = -P_{max}\, z\, F\nu\, ([Ba]_o/(\exp(\nu) - 1) + [Ba]_i/(\exp(-\nu) - 1))\, (1/(1 + \exp(-(V - V_h)/k)))^2 \quad (1)$$

with I being the I_{Ba} at the time the I–V was calculated (averaged over 7–8 ms after depolarization); P_{max} the maximum permeability; $\nu = zFV/(RT)$, with z being 2, F the Faraday constant, R the universal gas constant, T the absolute temperature, and V the membrane potential. $[Ba]_i$ (set at 50 nM) and $[Ba]_o$ denote the intracellular and extracellular Ba^{2+} concentration, respectively.

In vivo recordings from VCN spherical BCs. Juxtacellular single-unit recordings were acquired *in vivo* from spherical BCs in the anteroventral cochlear nucleus (AVCN) from 6 $\alpha_2\delta3^{+/+}$ and 4 $\alpha_2\delta3^{-/-}$ mice 5–8 weeks old. Animals were anesthetized with an initial intraperitoneal injection of a mixture of ketamine hydrochloride (180 mg/kg body weight; Ketavet, Pfizer) and xylazine hydrochloride (7 mg/kg body weight; Rompun, Bayer), and anesthesia was maintained by additional subcutaneous application of one-third of the initial dose (typically 60 min intervals). The AVCN was approached dorsally with the animal tilted at 14–18° to the midsagittal plane. Body temperature was kept between 37.5° and 38.5°C by positioning the animal on a temperature-controlled heating pad. The protocol for acoustic stimulation and single-unit recording was described previously (Dietz et al., 2012). Briefly, stimuli were generated by custom-written MATLAB software (MathWorks) at a sampling rate of 97.7 kHz. The stimuli were transferred to a real-time processor (RP2.1, Tucker-Davis Technologies), D/A converted and sent to custom-made earphones (acoustic transducer: DT 770 pro, Beyer Dynamics). Three stimulation protocols were used: (1) The excitatory response areas of extracellularly recorded single units were measured by random presentation of pure tone pulses (100 ms duration, 5 ms rise-fall time, 200 ms interstimulus interval) within a predefined matrix of frequency/intensity pairs (20 frequencies on a logarithmic scale, 9 intensity levels on a linear scale, 4–5 repetitions). From these data, characteristic frequency (CF, stimulus frequency to which the unit is most sensitive) and threshold were obtained and used for the next protocol: (2) Temporal response properties of single units were measured by presenting 100 ms tone bursts at CF 20 dB above threshold. Peristimulus time histograms were generated from these datasets and served for evaluation of the neurons' temporal response patterns, spike latencies, jitter of evoked responses, and firing rates. First spike latency (FSL) was determined as the median value of the time between the onset of the stimulus and the first evoked spike, calculated for each repetition, jitter of the responses as the SD of the FSL. (3) Neuronal spontaneous discharge activity was acquired in absence of acoustic stimulation and used to obtain average firing rate and mean waveform of the recorded signals. After multiunit mapping, juxtacellular single-unit recordings were performed using 8-15 MΩ glass micropipettes. The acquired voltage signals were preamplified (Neuroprobe 1600, A-M Systems), bandpass filtered (0.3–7 kHz), and further amplified (PC1, Tucker-Davis Technologies). Voltage traces were then digitized at a sampling rate of 97.7 kHz (RP2.1, Tucker-Davis Technologies) and stored for offline analysis using a custom-written MATLAB software. Three criteria were used to classify single-unit recordings: (1) changes in the spike height did not exceed 20%, (2) uniform waveforms (Englitz et al., 2009; Typlt et al., 2010), and (3) signal-to-noise ratio at least 6:1. Spherical BCs of the AVCN were identified by the complex waveform of the recorded discharges.

Auditory discrimination learning. Female, 7- to 9-week-old $\alpha_2\delta3^{+/+}$ and $\alpha_2\delta3^{-/-}$ mice were trained in one daily session for 20 d in a two-compartment shuttle-box using a go/no-go avoidance discrimination learning procedure (Kurt and Ehret, 2010; Kurt et al., 2012a). A training session comprised 60 trials (i.e., 30 presentations of each conditioned stimulus). Mice had to cross the hurdle (go response) in response to tones of a given sound (positively reinforced conditioned stimulus, CS+) or to stay in the compartment where they were (no-go response) in response to another sound (negatively reinforced conditioned stimulus, CS−). For pure tone (PT) discrimination learning, a 12 kHz tone should initiate a go-response (CS+), whereas a 7 kHz tone should lead to a no-go-response (CS−). For the amplitude-modulated (AM) tone discrimination learning task, mice had to discriminate between 20 Hz (CS+) and 40 Hz (CS−) AM pure tones, both with carrier frequencies of 12 kHz. All tones were 70 ± 5 dB SPL and above the hearing threshold. Electrical foot shocks of 70–120 μA applied through the floor grid served as unconditioned stimuli (UCS). The UCS level was adjusted individually to achieve a mild escape response. Mice learned to avoid the UCS by crossing the hurdle within 4 s after the onset of one of the sounds to be discriminated. The animals could show four types of responses: (1) Hurdle crossing within 4 s after onset of the CS+ was considered a "hit" (conditioned response CR+). The CS+ presentation was stopped as soon as the hurdle was crossed and no UCS was delivered. (2) A "miss" was noted when the animal did not cross the hurdle within 4 s after the onset of the CS+ and the CS+ was continued together with an UCS presentation for maximally another 4 s to motivate the animal to cross the hurdle. (3) A "false alarm" (CR−) was noted when the animal crossed the hurdle during the 4 s CS− presentation. In that case, the animal received a UCS (0.5 s of duration) in the compartment to which it had crossed. (4) A "correct rejection" was noted when the animal remained in the compartment during the 4 s presentation of the CS−. Group means (±SD) were calculated from individual CR+ and CR− response rates (hits and false alarms), and significance levels of CR+ and CR− rates at a given training session were analyzed using the Mann–Whitney U test.

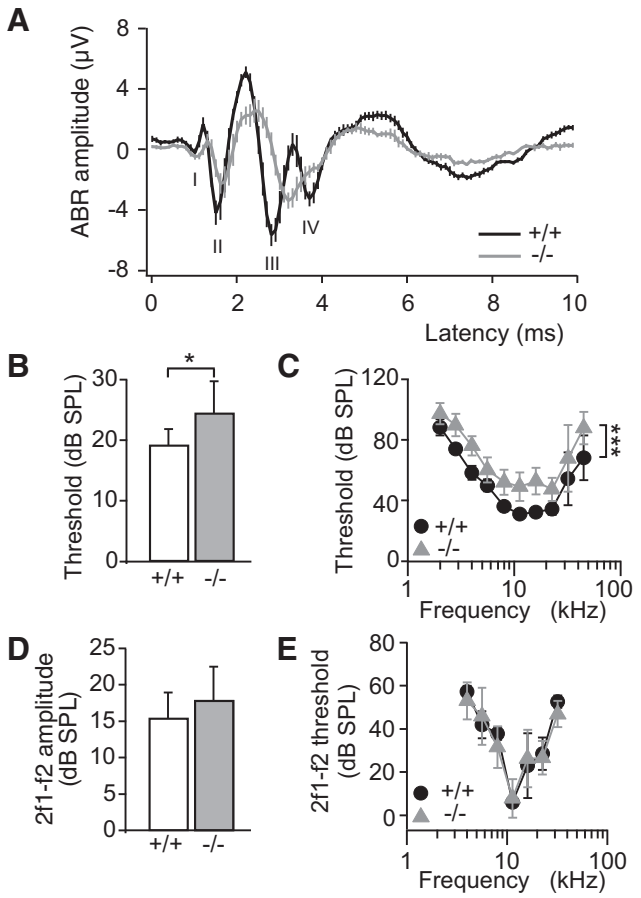

Figure 3. ABRs and DPOAEs. ***A***, Averaged ABR waveforms to click stimuli at 40 dB above threshold (mean ± SEM) showed a reduced amplitude of wave II and distortion of waves III and IV in $\alpha_2\delta3^{-/-}$ mice ($n = 10$ ears) compared with $\alpha_2\delta3^{+/+}$ ($n = 10$ ears). ***B***, The ABR threshold (mean ± SD) for click stimuli was increased in $\alpha_2\delta3^{-/-}$ mice ($n = 12$; $\alpha_2\delta3^{+/+}$, $n = 14$). $p = 0.017$ (t test). ***C***, ABR thresholds (mean ± SD) as a function of stimulus tone frequency were significantly increased in $\alpha_2\delta3^{-/-}$ mice ($n = 12$; $\alpha_2\delta3^{+/+}$, $n = 14$). ***$p < 0.001$ (2-way ANOVA, effect of genotype). ***D***, Unchanged DPOAE maximum amplitudes at f1 = 9.1 kHz, L1 = 50 dB SPL, f2 = 11.3 kHz, and L2 = 40 dB SPL gave a similar rating for integrity of OHC function in $\alpha_2\delta3^{+/+}$ ($n = 7$) and $\alpha_2\delta3^{-/-}$ mice ($n = 6$). ***E***, DPOAE thresholds (dB SPL ± SD) were similar for both genotypes.

Results

Startle responses of $\alpha_2\delta3^{-/-}$ mice

Because a decreased SR has been reported for $\alpha_2\delta3^{-/-}$ mice, we analyzed both acoustic and tactile SR. Acoustic SR amplitudes were measured at 75–115 dB SPL (Fig. 2*A*). Both $\alpha_2\delta3^{+/+}$ and

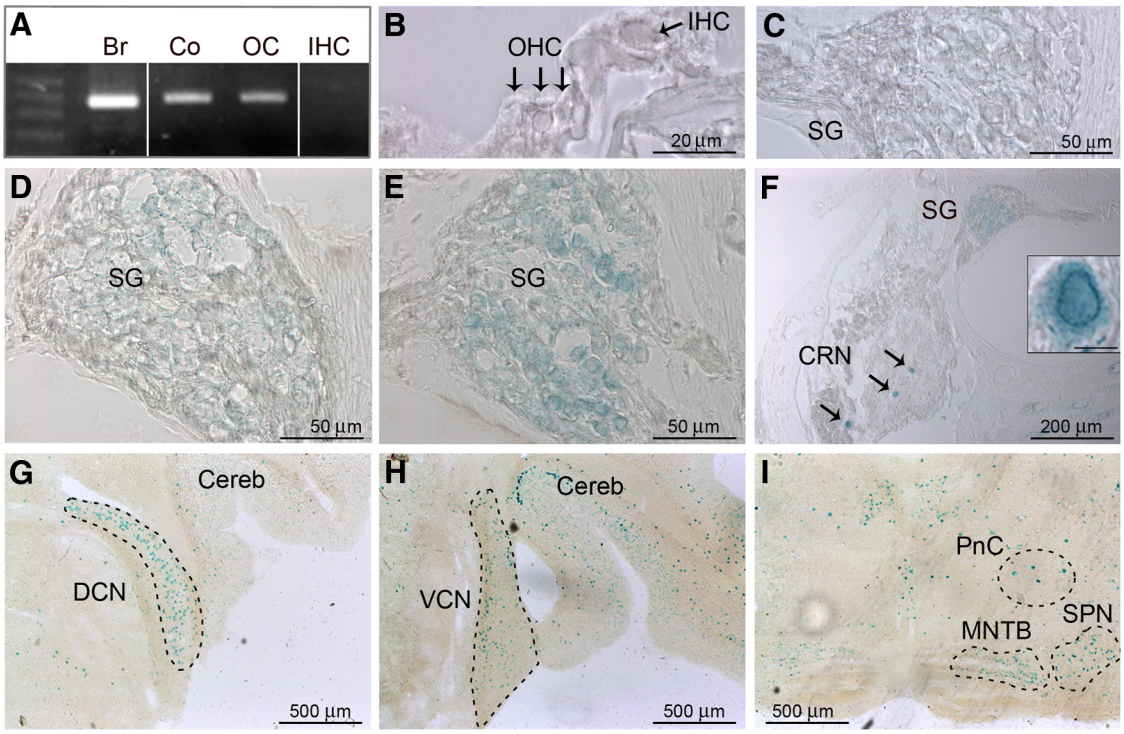

Figure 4. $\alpha_2\delta3$ expression in the cochlea and medullary brainstem. ***A***, $\alpha_2\delta3$-specific transcripts (356 bp) were detected in brain (Br), cochlea (Co), and organ of Corti (OC), but not in IHCs of 3-week-old mice by nested PCR. ***B–F***, LacZ staining in cochlear sections of adult $\alpha_2\delta3^{-/-}$ mice using the reporter function of the construct (***B***, ***D–F***) and of adult $\alpha_2\delta3^{+/+}$ SG from midbasal/basal cochlea as a negative control (***C***). No $\alpha_2\delta3$ expression in IHCs and OHCs of the OC (***B***, arrows) but in apical (***D***) and more intensely in basal SG neurons (***E***) as well as in the large cochlear root neurons scattered in the auditory nerve (CRN; arrows in ***F*** and inset). Scale bar, inset: 10 μm. ***G–I***, LacZ staining in brainstem sections of adult $\alpha_2\delta3^{-/-}$ mice revealed $\alpha_2\delta3$ expression in neurons of the dorsal cochlear nucleus (DCN; ***G***), the VCN (***H***), the cerebellum (Cereb; ***G***, ***H***), the medial nucleus of the trapezoid body (MNTB; ***I***), the superior paraolivary nucleus (SPN; ***I***), and in giant neurons of the caudal pontine reticular formation (PnC; ***I***).

$\alpha_2\delta3^{-/-}$ mice showed a monotonic increase of startle amplitude with increasing SPL; however, $\alpha_2\delta3^{-/-}$ mice had lower SR amplitudes. Startle threshold was higher in $\alpha_2\delta3^{-/-}$ (84.2 ± 1.6 dB SPL) than controls (79.9 ± 1.6 dB SPL). Importantly, the slope of the SR curve as a function of SPL was significantly less steep in $\alpha_2\delta3^{-/-}$, which mostly accounts for the different acoustic SR phenotype.

The acoustic SR is modulated by acoustic stimuli preceding the startle stimulus (Plappert et al., 2006). One form of modulation is the PPI that involves the cochlear nuclear complex, the inferior and superior colliculus, the pedunculopontine tegmental nucleus, and the caudal pontine reticular formation (PnC). In both genotypes, the amount of PPI similarly increased with prepulse SPL (Fig. 2*B*). Because startle amplitudes to 105 dB SPL were relatively small in $\alpha_2\delta3^{-/-}$, their PPI values were additionally compared with those of $\alpha_2\delta3^{+/+}$ mice responding to startle stimuli of only 85 dB SPL (mean response: 88.9% of that of $\alpha_2\delta3^{-/-}$ mice at 105 dB). Again, there was no significant effect of the genotype on PPI (Fig. 2*B*). Tactile stimuli can also elicit a SR. Unexpectedly, tactile SR amplitudes, elicited by air puffs, were on average 7.9-fold higher in $\alpha_2\delta3^{-/-}$ than in $\alpha_2\delta3^{+/+}$ mice (Fig. 2*C*). Each single $\alpha_2\delta3^{-/-}$ mouse had a higher mean tactile startle than the $\alpha_2\delta3^{+/+}$ littermates.

Auditory function in $\alpha_2\delta3^{-/-}$ mice

A reduced acoustic SR can imply hearing impairment since startle and auditory pathways share some components such as hair cells and SG neurons (Fig. 1). To test whether the lack of $\alpha_2\delta3$ impairs signal transmission, we recorded ABRs in 4-week-old mice. ABR waveforms among $\alpha_2\delta3^{-/-}$ mice were more variable in timing and amplitude than those in $\alpha_2\delta3^{+/+}$. Averaged ABR waveforms for click stimuli 40 dB above threshold revealed considerable differences between genotypes (Fig. 3*A*). In $\alpha_2\delta3^{-/-}$ mice, the amplitude of wave II was significantly reduced by 44%, and the positive peak of wave III and the negative peak of wave IV were missing or overlapping. The timing of late waves (>5 ms) was similar in both genotypes, although their amplitudes were reduced in the mutants (Fig. 3*A*). These findings indicate impaired synaptic transmission in the CN and likely in subsequent auditory brainstem stations.

Click-ABR thresholds were significantly increased by 5.2 dB in $\alpha_2\delta3^{-/-}$ mice compared with $\alpha_2\delta3^{+/+}$ (Fig. 3*B*; 24.6 ± 6.8 dB SPL vs 19.4 ± 3.2 dB SPL). Averaged pure tone ABR thresholds were increased across the entire frequency range in $\alpha_2\delta3^{-/-}$ (Fig. 3*C*). Hearing function was further investigated by measuring DPOAEs, an objective indicator of OHC electromotility (Fig. 3*D*,*E*). DPOAE maximum amplitudes at f2 = 11.3 kHz and L1 = 50 dB SPL (Fig. 3*D*; $\alpha_2\delta3^{+/+}$: 15.6 ± 3.4 dB SPL; $\alpha_2\delta3^{-/-}$: 18 ± 4.6 dB SPL) and DPOAE thresholds of the DPOAE growth function were similar in both genotypes (Fig. 3*E*), indicating normal cochlear mechanics and OHC function upon $\alpha_2\delta3$ loss. Together, ablation of $\alpha_2\delta3$ impairs the function of the auditory periphery and the brainstem yet does not affect OHC function.

$\alpha_2\delta3$ expression in the cochlea and medullary brainstem

RT-PCR revealed $\alpha_2\delta3$-specific transcripts (356 bp) in brain, cochlea, and organ of Corti. Whereas $\alpha_2\delta3$ was never found in mature IHCs (≥P18) by a nested PCR approach (Fig. 4*A*), it was occasionally detected in P6 IHCs, suggesting very low expression at this age. $\alpha_2\delta3$ expression was also assessed by LacZ staining for

the *CACNA2D3* reporter construct in cochlear and brainstem sections from 4- to 5-week-old $\alpha_2\delta3^{-/-}$ mice. LacZ staining was negative in the organ of Corti (Fig. 4*B*) but positive in SG neurons (Fig. 4*D*,*E*). A negative control of LacZ staining is shown for basal SG from $\alpha_2\delta3^{+/+}$, which are devoid of the reporter construct (Fig. 4*C*). $\alpha_2\delta3$ expression was less intense in the apical compared with the basal cochlear turn (Fig. 4*D*,*E*). This result was confirmed in P6 $\alpha_2\delta3^{+/+}$ mice by *in situ* hybridization using a specific $\alpha_2\delta3$ riboprobe (data not shown).

Interestingly, strong $\alpha_2\delta3$ expression was found in cochlear root (CR) neurons (Fig. 4*F*) of the startle pathway, which are localized within the auditory nerve close to the brainstem and belong to the cochlear nuclear complex (compare Fig. 1). In the adult brainstem, $\alpha_2\delta3$ expression was detected in the main nuclei of the central auditory and startle pathways, such as the dorsal cochlear nucleus (Fig. 4*G*), the VCN (Fig. 4*H*), the superior olivary complex (shown for the paraolivary nucleus, superior paraolivary nucleus, and the medial nucleus of the trapezoid body; Fig. 4*I*), and the caudal PnC (Fig. 4*I*).

Lack of $\alpha_2\delta3$ does not affect expression and function of $Ca_v1.3$ channels in IHCs

Maturation of IHCs and mature IHC synaptic transmission rely on Ca^{2+} influx through $Ca_v1.3$ channels (Platzer et al., 2000; Brandt et al., 2003). To test whether lack of $\alpha_2\delta3$ affects $Ca_v1.3$ function in IHCs, VGCC currents were recorded in IHCs before hearing onset (P6–P9) and thereafter (P16–P19), using 10 mM Ba^{2+} as charge carrier (I_{Ba}). Representative Ba^{2+} inward currents elicited by 8 ms depolarization steps from −78 mV were similar in mature IHCs of $\alpha_2\delta3^{+/+}$ and $\alpha_2\delta3^{-/-}$ mice (Fig. 5*A*,*B*). Averaged I–V curves for 12 $\alpha_2\delta3^{+/+}$ and 14 $\alpha_2\delta3^{-/-}$ IHCs obtained by taking mean I_{Ba} during the last millisecond of the depolarizing step are shown in Figure 5*C*. IHC Ca^{2+} currents normally peak at P6, which we also observed (for I_{Ba}) in $\alpha_2\delta3^{+/+}$ and $\alpha_2\delta3^{-/-}$ IHCs. Mean peak I_{Ba} normalized by cell capacitance (I_{Ba} density) was significantly reduced by 19% in immature $\alpha_2\delta3^{-/-}$ IHCs (69.1 ± 14.6 pA/pF; $\alpha_2\delta3^{+/+}$: 84.4 ± 16.7 pA/pF; Fig. 5*D*). There was a similar tendency for a smaller I_{Ba} density in mature $\alpha_2\delta3^{-/-}$ IHCs ($\alpha_2\delta3^{-/-}$: 18.5 ± 4.2 pA/pF; $\alpha_2\delta3^{+/+}$: 22.4 ± 5.5 pA/pF; $p = 0.053$, Fig. 5*D*; see also averaged I–V curves in Fig. 5*C*). I–V curves were analyzed for voltages of half-maximum I_{Ba} activation (V_h) and slope. V_h showed a tendency to more positive values in IHCs of $\alpha_2\delta3^{-/-}$ compared with $\alpha_2\delta3^{+/+}$ at P6–P9 ($\alpha_2\delta3^{+/+}$: −33.8 ± 3.7 mV; $\alpha_2\delta3^{-/-}$: −30.2 ± 6.0 mV, $p = 0.062$), and was significantly increased in P16–P19 $\alpha_2\delta3^{-/-}$ mice compared with wild-type ($\alpha_2\delta3^{+/+}$: −33.1 ± 3.1 mV; $\alpha_2\delta3^{-/-}$: −29.1 ± 3.5 mV; Fig. 5*E*). The slope of I_{Ba} activation was unaffected by the lack of $\alpha_2\delta3$ in prehearing and posthearing IHCs (Fig. 5*F*).

Because $\alpha_2\delta$ subunits are involved in trafficking α_1 subunits to the plasma membrane, we tested whether targeting or clustering of $Ca_v1.3$ was affected by $\alpha_2\delta3$ deletion. Immunofluorescence labeling of cochlear cryosections revealed $Ca_v1.3$-positive dots at the basolateral pole of IHCs that were in close apposition with synaptic ribbons in either genotype (Fig. 5*G*). There was no significant difference in the number of $Ca_v1.3$-positive clusters per IHC ($\alpha_2\delta3^{+/+}$: 23.1 ± 6.8, $n = 7$; $\alpha_2\delta3^{-/-}$: 17.7 ± 9.0, $n = 9$, $p = 0.19$) as well as ribbons ($\alpha_2\delta3^{+/+}$: 17.5 ± 3.7, $n = 8$; $\alpha_2\delta3^{-/-}$: 14.8 ± 5.5, $n = 9$, $p = 0.24$). Together, the lack of $\alpha_2\delta3$ causes a small reduction of I_{Ba} in immature IHCs and a small shift of its voltage dependence in mature IHCs but does not affect $Ca_v1.3$ protein expression and targeting to ribbon synapses.

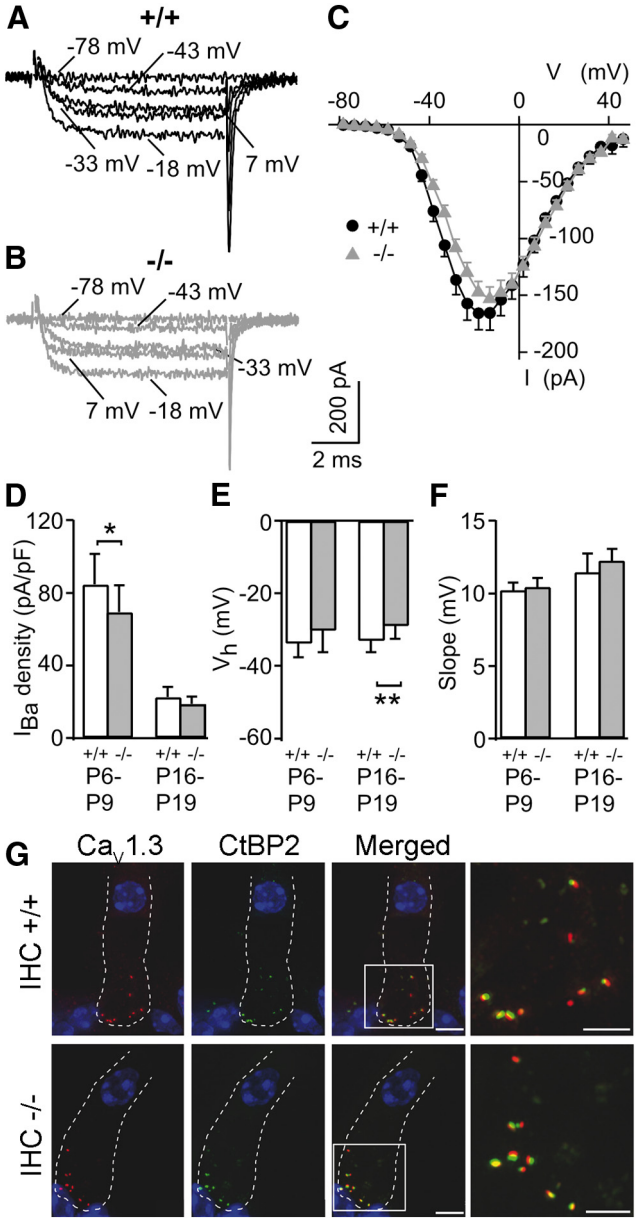

Figure 5. Whole-cell Ba^{2+} currents and localization of $Ca_v1.3$ channels in IHCs. ***A–F***, Ba^{2+} currents (I_{Ba}) in IHCs of $\alpha_2\delta3^{+/+}$ and $\alpha_2\delta3^{-/-}$ mice before (P6–P9; $n = 15$, $n = 14$) and after hearing onset (P16–P19; $n = 12$, $n = 14$). ***A***, ***B***, Representative I_{Ba} traces of a P18 $\alpha_2\delta3^{+/+}$ IHC (***A***) and a P16 $\alpha_2\delta3^{-/-}$ IHC (***B***) in response to 8 ms depolarizing steps to the voltages indicated. ***C***, Averaged I–V curves ± SD for both genotypes. For clarity, SD is plotted in one direction only (−SD or +SD). ***D***, Averaged peak I_{Ba} density ± SD was reduced in $\alpha_2\delta3^{-/-}$ IHCs compared with $\alpha_2\delta3^{+/+}$ at P6–P9 (*t* test, $p = 0.015$), with a tendency of smaller values in $\alpha_2\delta3^{-/-}$ versus $\alpha_2\delta3^{+/+}$ IHCs after hearing onset ($p = 0.053$). ***E***, The average voltage of half-maximum I_{Ba} activation (V_h) ± SD was similar between genotypes at P6–P9 ($p = 0.062$) and increased by 4.1 mV in $\alpha_2\delta3^{-/-}$ at P16–P19 ($p < 0.01$). ***F***, Slope factors of I_{Ba} activation curves ± SD were similar in $\alpha_2\delta3^{+/+}$ and $\alpha_2\delta3^{-/-}$ mice before ($p = 0.23$) and after hearing onset ($p = 0.071$). ***G***, $Ca_v1.3$ (red) and CtBP2/RIBEYE immunolabeling (green) of cochlear cryosections revealed a similar dot-like staining at the IHC basolateral membrane of adult $\alpha_2\delta3^{+/+}$ (top row) and $\alpha_2\delta3^{-/-}$ (bottom row) mice, with extensive colocalization (merged and enlargements: yellow dots). Nuclei were stained in blue with DAPI. Scale bars, 5 μm; in enlargement, 2 μm.

Expression density of $Ca_v2.1$ channels is reduced in spiral ganglion neurons of $\alpha_2\delta3^{-/-}$ mice

As IHC ribbon synapses, the first synapses along the auditory pathway, appeared to be unaffected by the lack of $\alpha_2\delta3$, we ana-

lyzed SG neurons, which strongly express $\alpha_2\delta3$ mRNA (Fig. 4*D–F*). We postulated that $\alpha_2\delta3$ subunits are coassembled with the α_1 subunits $Ca_v2.1$ and $Ca_v2.2$ at ANF terminals contacting VCN cells. Because the contribution of $Ca_v2.1$ dominates over $Ca_v2.2$ regarding (1) presynaptic Ca^{2+} currents in P9–P11 axon terminals (85% mediated by $Ca_v2.1$) (Lin et al., 2011) and (2) evoked postsynaptic responses in juvenile VCN BCs (>80% mediated by $Ca_v2.1$) (Oleskevich and Walmsley, 2002), we analyzed $Ca_v2.1$ immunolabeling in the adult cochlea (Fig. 6) and brainstem (Fig. 7). In $\alpha_2\delta3^{+/+}$ mice, SG neurons showed $Ca_v2.1$ dot-like immunolabeling that accumulated in the soma membrane (Fig. 6*A*, arrow). $Ca_v2.1$-positive puncta were also seen in the cytoplasm and in neurites. SG neurons from apical cochlear turns of $\alpha_2\delta3^{+/+}$ mice showed less dot-like $Ca_v2.1$ labeling than those from basal turns (Fig. 6*A*,*B*), a tonotopic difference that was also observed in $\alpha_2\delta3^{-/-}$ mice (Fig. 6*C*,*D*). However, the amount of $Ca_v2.1$ immunolabeling was significantly reduced in all cochlear turns of $\alpha_2\delta3^{-/-}$ (Fig. 6*C*,*D*) compared with the respective locations in $\alpha_2\delta3^{+/+}$ mice (Fig. 6*A*,*B*). This was confirmed by quantitative analysis of the number of $Ca_v2.1$-positive dots per SG neuron in cochlear cryosections of 4 animals of each genotype (Fig. 6*E*). Concomitantly, the increasing gradient of $Ca_v2.1$ protein expression in $\alpha_2\delta3^{+/+}$ SG neurons from apex to base reflected that of LacZ expression under the *CACNA2D3* promoter (Fig. 4*D*,*E*).

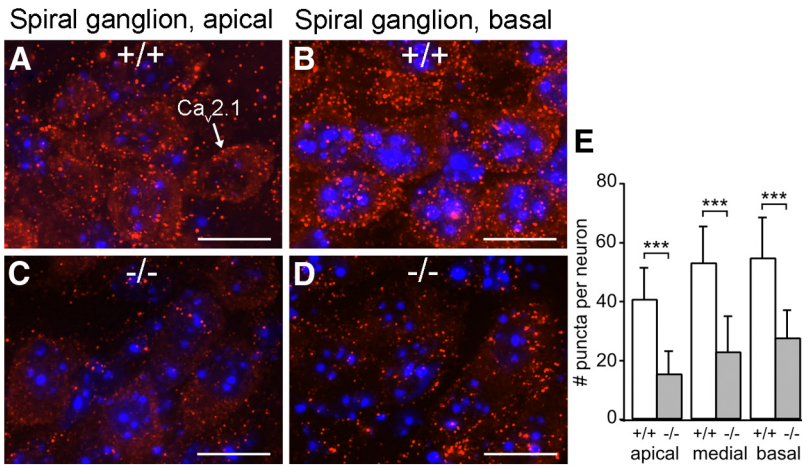

Figure 6. $Ca_v2.1$ expression in SG neurons. ***A–D***, Immunolabeling of cochlear cryosections (maximum intensity projection over 6 μm stacks) revealed punctate $Ca_v2.1$ staining patterns accumulating in membranes of SG neurons of $\alpha_2\delta3^{+/+}$ (***A***, ***B***) and $\alpha_2\delta3^{-/-}$ (***C***, ***D***) mice. In both genotypes, there was an increase of immunopositive puncta from the cochlear apex to the base. $\alpha_2\delta3^{-/-}$ SG neurons showed a markedly reduced $Ca_v2.1$ expression in the apical (***C***) and the basal turn (***D***) compared with the corresponding cochlear location in $\alpha_2\delta3^{+/+}$ (***A***, ***B***). ***E***, Statistical analysis of the average number of puncta per SG neuron ± SD for the apical, medial, and basal cochlear part of either genotype, respectively. Number of slides/number of neurons analyzed: $\alpha_2\delta3^{+/+}$: apical, 7/40; medial, 6/41; basal, 7/37; $\alpha_2\delta3^{-/-}$: apical, 7/33; medial, 7/39; basal, 7/37. ***$p < 0.001$ (Wilcoxon rank test). Nuclei were stained in blue with DAPI. Scale bars, 10 μm.

Lack of $\alpha_2\delta3$ changes the size of synaptic boutons in the VCN

ABR waveforms of $\alpha_2\delta3^{-/-}$ mice (compare Fig. 3*A*) indicated a hearing impairment that was most likely due to defective synaptic transmission from ANFs to cochlear nuclei and further in the brainstem. The reduced somatic $Ca_v2.1$ expression in $\alpha_2\delta3^{-/-}$ SG neurons is in line with this idea. We asked whether $Ca_v2.1$ expression was also altered at ANF terminals contacting BCs in the VCN (the "endbulb of Held" synapses). More $Ca_v2.1$-immunopositive dots were found at the membrane (implying presynaptic or postsynaptic localization) and in the cytoplasm (implying postsynaptic localization) of $\alpha_2\delta3^{+/+}$ BCs (Fig. 7*A*, green), but fewer in BCs of $\alpha_2\delta3^{-/-}$ mice (Fig. 7*B*). To distinguish between presynaptic and BC somatic (postsynaptic) $Ca_v2.1$ channels, brainstem slices were colabeled for vesicular glutamate transporter 1 (VGLUT1; red), a marker for the glutamatergic ANF terminals, presumably reflecting active zones. Few $Ca_v2.1$-positive dots were included in the bigger VGLUT1-positive boutons on $\alpha_2\delta3^{+/+}$ BC somata, indicating presynaptic $Ca_v2.1$ channels (Fig. 7*A*, arrows), which were often absent in $\alpha_2\delta3^{-/-}$ BCs (Fig. 7*B*). However, because of protein crowding and epitope masking of Ca_v2 channels at active zones (Müller et al., 2010), which hinders antibody binding, our data likely severely underestimate the number of ANF presynaptic Ca^{2+} channel clusters of both genotypes.

VGLUT1-positive boutons at $\alpha_2\delta3^{-/-}$ BC somata (Fig. 7*A*) differed morphologically from those in $\alpha_2\delta3^{+/+}$ mice (Fig. 7*B*) by their significantly higher proportion of smaller boutons, as evident from cumulative distributions and median values ($\alpha_2\delta3^{-/-}$: 0.66 μm^2; $\alpha_2\delta3^{+/+}$: 1.44 μm^2; Fig. 7*E*). VGLUT1-positive boutons were also analyzed at ANFs terminating on CR neurons (Fig. 7*C*,*D*). Again, a significant reduction of the median value of VGLUT1-positive ANF bouton area contacting CR somata was found in $\alpha_2\delta3^{-/-}$ animals (0.54 μm^2, $\alpha_2\delta3^{+/+}$: 1.10 μm^2; Fig. 7*F*).

To investigate the ultrastructure of endbulbs of Held, we performed electron microscopy in thin VCN sections where endbulbs were identified by anti-VGLUT1 labeling (Fig. 7*G–J*). Endbulbs at $\alpha_2\delta3^{-/-}$ BCs were smaller and had less intercellular channel cisterns (Fig. 7*H*) compared with $\alpha_2\delta3^{+/+}$ (Fig. 7*G*, asterisks). Giant endbulbs extending over ≥12 μm were occasionally observed in $\alpha_2\delta3^{+/+}$ mice (Fig. 7*I*) but were never found in $\alpha_2\delta3^{-/-}$ animals. A quantitative analysis of bouton areas, excluding $\alpha_2\delta3^{+/+}$ giant endbulbs, was performed. Box-and-whisker plots of the bouton areas of each individual animal (Fig. 7*J*, thin bars) and for the $\alpha_2\delta3^{+/+}$ and $\alpha_2\delta3^{-/-}$ groups (Fig. 7*J*, broad bars) indicated smaller bouton areas for $\alpha_2\delta3^{-/-}$ (median 1.7 μm^2) versus $\alpha_2\delta3^{+/+}$ animals (median 5.8 μm^2) at the electron microscopic level. Together, these findings indicate that $\alpha_2\delta3$ loss reduces the amount of $Ca_v2.1$ channels at ANF terminals and BC somata and decreases the size of ANF terminals.

***In vivo* recordings at the ANF–BC synapse**

To analyze functional consequences of reduced presynaptic Ca^{2+} channels and smaller endbulb of Held synapses in $\alpha_2\delta3$-deficient mice, juxtacellular *in vivo* recordings of sound-evoked activity were performed at ANF–BC synapses. The complex waveform was used as a criterion to identify BCs in the rostral VCN (Englitz et al., 2009; Typlt et al., 2010), and the extracellularly recorded signal was decomposed into presynaptic and postsynaptic components (Fig. 8*A*). Spontaneous activity of single units did not differ between genotypes (Fig. 8*B*,*C*), whereas tone burst-evoked activity was reduced in $\alpha_2\delta3^{-/-}$ (Fig. 8*B*,*C*). Rate-level functions of tone burst-evoked activity at CF revealed smaller mean firing rates in $\alpha_2\delta3^{-/-}$ for intensities ≥20 dB SPL above threshold (Fig. 8*C*). Maximum firing rates at best frequency (i.e., the frequency in the response area causing the highest spike discharge rate,

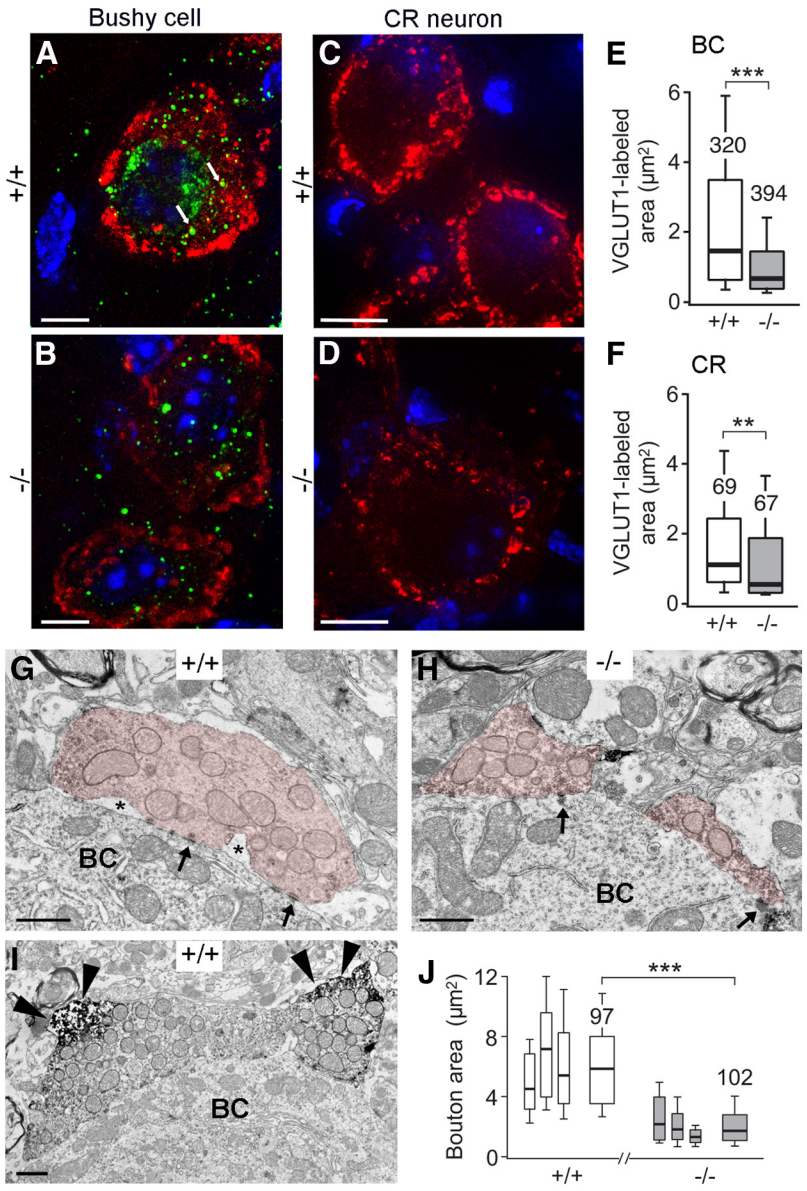

Figure 7. ANF synaptic boutons contacting BCs and cochlear root (CR) neurons. ***A–F***, Light microscopic analysis revealed smaller ANF terminals on VCN BCs and on CR neurons in brainstem sections of $\alpha_2\delta3^{-/-}$ mice. ***A***, ***B***, Double immunolabeling of VCN slices revealed dot-like $Ca_v2.1$ channels (green) and VGLUT1-positive ANF terminals (presumably representing active zones in the endbulbs of Held, red) on BC somata. ***A***, A typical example of an $\alpha_2\delta3^{+/+}$ BC showed sparse overlap of $Ca_v2.1$-positive dots with VGLUT1 immunoreactivity (arrows). ***B***, Two typical $\alpha_2\delta3^{-/-}$ BCs displayed fewer $Ca_v2.1$-positive puncta than $\alpha_2\delta3^{+/+}$ BCs, which did not overlap with VGLUT1. VGLUT1-labeled boutons were less intense in $\alpha_2\delta3^{-/-}$ than in $\alpha_2\delta3^{+/+}$ BCs. ***C***, ***D***, ANF terminals on CR neurons, as revealed by anti-VGLUT1 staining (red), were larger in $\alpha_2\delta3^{+/+}$ mice. Scale bars: ***A***, ***B***, 5 μm; ***C***, ***D***, 10 μm. Cell nuclei were stained in blue with DAPI. ***E***, ***F***, Box-and-whisker plots of VGLUT1-positive (active zone) areas in $\alpha_2\delta3^{+/+}$ and $\alpha_2\delta3^{-/-}$ BCs (***E***) and CR neurons (***F***). Boxes represent the 25th-75th percentiles, the median (horizontal bar), and 10th-90th percentiles (whiskers). Numbers at bars depict the number of boutons analyzed. ***$p < 0.001$ (Wilcoxon rank test). **$p < 0.01$ (Wilcoxon rank test). ***A–D***, Maximum intensity projections of deconvoluted *z*-stack images. ***E***, ***F***, Data were obtained from conventional fluorescence images. ***G–J***, High-magnification electron micrographs of VGLUT1-immunoreactive ANF terminals (***G***, ***H***, pink shading) on BC somata of $\alpha_2\delta3^{+/+}$ (***G***, ***I***) and $\alpha_2\delta3^{-/-}$ mice (***H***). ***G***, ***H***, Several postsynaptic densities were present (arrows). $\alpha_2\delta3^{+/+}$ endbulbs of Held were larger, contained more mitochondria, and had more intercellular channel cisterns (asterisks). ***I***, Giant endbulbs extending over ≥12 μm were typical for $\alpha_2\delta3^{+/+}$ animals but were never observed in $\alpha_2\delta3^{-/-}$. Boutons were VGLUT1-positive, as indicated by arrowheads in ***I***. Scale bars, 1 μm. ***J***, Box-and-whisker plots for bouton area sizes of $\alpha_2\delta3^{+/+}$ mice (thin white boxes, $n = 3$) and $\alpha_2\delta3^{-/-}$ mice (thin gray boxes, $n = 3$), each representing between 29 and 34 boutons. Broad boxes represent pooled data. ***$p < 0.001$ (Wilcoxon rank test).

typically one-half octave below CF) were also significantly lower in $\alpha_2\delta3^{-/-}$ mice (Fig. 8*D*). First spike latency (FSL) was significantly increased by 1.0 ms, and the jitter showed a tendency toward larger values in $\alpha_2\delta3^{-/-}$ without reaching significance. These results showed impaired synaptic transmission with reduced rate-level functions at best frequency for ≥20 dB above threshold and a delayed first spike latency at the endbulb of Held synapses in $\alpha_2\delta3^{-/-}$ mice.

Auditory discrimination learning

To assess the consequences of impaired ANF synapse performance, such as reduced postsynaptic spike rates and increased latency, on the discrimination of temporally structured tones, we performed auditory discrimination learning tasks. Auditory discrimination learning, which involves several cortical and subcortical auditory stations, is a reliable and suitable method for mouse phenotyping (Kurt et al., 2012a; b). We applied a foot shock-motivated go/no-go shuttle-box paradigm to test whether $\alpha_2\delta3^{-/-}$ mice are able to discriminate (1) in the spectral domain, pure tones of 7 kHz versus 12 kHz (PT discrimination) and (2) in the temporal domain, amplitude-modulated tones with 20 Hz versus 40 Hz modulation frequency (AM discrimination) but the same carrier frequency (12 kHz). The learning curves of $\alpha_2\delta3^{+/+}$ and $\alpha_2\delta3^{-/-}$ to PT discrimination showed changes in the animals' learning performance over 20 training sessions (Fig. 9*A*,*B*). Significant learning is indicated by the increase of the number of hits (CR+, hurdle crossings as conditioned responses to 12 kHz tones) relative to the number of false alarms (CR−, hurdle crossings to 7 kHz tones, to which the mice should stay in the actual compartment). Differences between CR+ and CR− were statistically evaluated for each training session. Starting at training session 2 ($\alpha_2\delta3^{+/+}$) and 5 ($\alpha_2\delta3^{-/-}$), mice performed significant PT discrimination up to the 20th training session (Fig. 9*A*,*B*), although $\alpha_2\delta3^{-/-}$ mice reached a lower performance level. For AM discrimination, results were totally different (Fig. 9*C*,*D*). From the sixth training session onwards, $\alpha_2\delta3^{+/+}$ significantly discriminated the different AM tones, as illustrated by the numbers of hits (CR+, hurdle crossings to the 20 Hz-AM tones) and false alarms (CR−, 40 Hz-AM tones; Fig. 9*C*). By contrast, $\alpha_2\delta3^{-/-}$ mice completely failed to discriminate for the entire training period of 20 d (Fig. 9*D*).

Discussion

Here we demonstrate deficits in auditory and acoustic startle processing of $\alpha_2\delta3^{-/-}$ mice. ABR waveforms were distorted from wave II to IV, reflecting impaired synaptic transmission at ANF synapses in the VCN and likely further up in

the auditory pathway. $\alpha_2\delta3^{-/-}$ mice learned to discriminate pure tones, but not temporally structured amplitude-modulated tones, whereas $\alpha_2\delta3^{+/+}$ performed well. Indeed, impaired synaptic transmission was demonstrated via *in vivo* recordings from ANF–BC synapses. At the cellular level, $\alpha_2\delta3^{-/-}$ mice displayed less $Ca_v2.1$ immunoreactivity in somata of SG neurons and ANF–BC synapses. Moreover, ANF terminals contacting BC (auditory pathway) or CR neurons (acoustic startle pathway) were smaller in size.

Synaptic transmission requires proper VGCC function. Auxiliary $\alpha_2\delta$ subunits are crucial for targeting the pore-forming subunits to the plasma membrane and can modulate their properties. Recent studies have identified specific roles of each $\alpha_2\delta$ isoform in structure and function that cannot be compensated by another one. Here, we analyzed the role of $\alpha_2\delta3$ with special emphasis on the auditory system, using a new mouse model with impaired acoustic SR. Acoustic SR and auditory pathway share common elements (i.e., cochlear mechanics, IHC transduction and synaptic transmission, and ANF signal generation and conduction), yet the two pathways differ in ANF synaptic transmission activating BCs (auditory pathway) or CR neurons (acoustic SR pathway, compare Fig. 1). We have analyzed the link between acoustic SR deficits and impaired auditory function of $\alpha_2\delta3$-deficient mice, such as increased ABR thresholds and reduced early ABR wave amplitudes. Startle threshold increase was similarly small (+4.3 dB) as the increase of the ABR threshold (+5.2 dB). Therefore, the markedly shallower input–output function of the acoustic SR must have resulted from a change in startle-specific stimulus processing rather than from the small increase in hearing threshold.

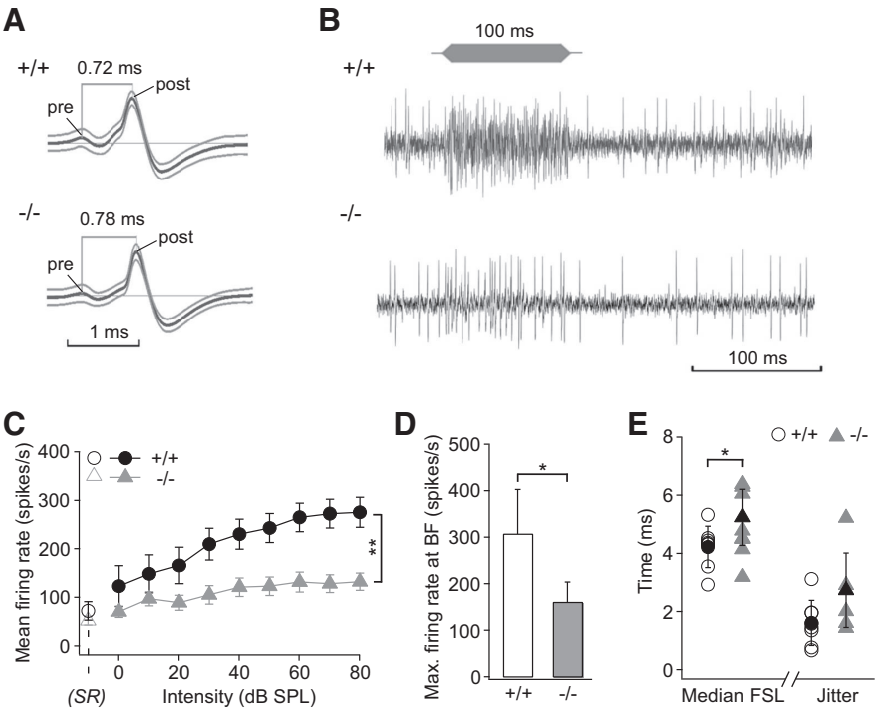

Figure 8. Juxtacellular *in vivo* recordings from BCs in the VCN. ***A***, The complex waveform of spontaneous discharge activity of two exemplary units (top, $\alpha_2\delta3^{+/+}$; bottom, $\alpha_2\delta3^{-/-}$) served as one criterion to identify BCs. Thick lines indicate the mean waveform for ≥2800 spikes; thin gray lines indicate ±SD. Juxtacellular spike signals can be decomposed into their presynaptic (pre) and postsynaptic component (post); the mean latency between the two is indicated. ***B***, Exemplary traces of tone-burst-evoked activity (20 dB above neuron's threshold, 100 ms tone burst indicated on top) and peristimulus spontaneous activity. ***C***, Mean firing rate ± SEM as a function of SPL of $\alpha_2\delta3^{+/+}$ and $\alpha_2\delta3^{-/-}$ BCs ($n = 9$, $n = 10$). There is reduced increase of discharge rates with increasing intensity at ≥20 dB above threshold in $\alpha_2\delta3^{-/-}$ mice (ANOVA with *post hoc* Newman–Keul's test; 20 dB, $p < 0.05$; 30 – 60 dB, $p < 0.01$; 70 – 80 dB, $p < 0.001$). Spontaneous firing rates (SR, open symbols on the left) did not differ between genotypes. ***D***, Maximum firing rate at best frequency (BF) was approximately twofold lower in $\alpha_2\delta3^{-/-}$ BCs (mean ± SD; $n = 10$, $n = 9$). $p < 0.05$ (*t* test). ***E***, Increased FSL (left; $p < 0.05$, *t* test) and jitter of FSL (right) to tone bursts in $\alpha_2\delta3^{-/-}$ mice. Tone bursts were presented at the units' characteristic frequency and 20 dB above threshold ($\alpha_2\delta3^{-/-}$, $n = 7$; $\alpha_2\delta3^{+/+}$, $n = 8$; respective black symbols: mean ± SD).

Intact DPOAEs in $\alpha_2\delta3^{-/-}$ animals indicate normal cochlear mechanics and integrity of OHCs, which amplify the acoustic signal. In turn, IHCs transform sound-induced depolarization into transmitter release, representing the first level of signal processing in both hearing and acoustic SR. Ablation of the auxiliary VGCC subunit $\beta2$ causes a 70% reduction of IHC Ca^{2+} currents and exocytosis, resulting in deafness (Neef et al., 2009). In contrast, robust Ba^{2+} currents (Fig. 5*A–C*) and colocalization of $Ca_v1.3$ channels with ribbons in $\alpha_2\delta3^{-/-}$ IHCs (Fig. 5*G*) suggest a retrocochlear origin of the hearing deficits and acoustic SR deficits in $\alpha_2\delta3^{-/-}$ mice. Although $\alpha_2\delta3$ expression was not detected in mature IHCs, we observed a small but significant reduction of I_{Ba} in immature and an increased V_h in mature $\alpha_2\delta3^{-/-}$ IHCs (Fig. 5*D*,*E*). Either immature IHCs express very little $\alpha_2\delta3$, which we could not consistently amplify with nested RT-PCR, or altered activity in SG or central auditory neurons indirectly affects I_{Ba} and V_h. Superior olivary complex neurons exert a transient inhibitory feedback on developing IHCs (Simmons, 2002) that interrupts their spiking activity (Glowatzki and Fuchs, 2000), and impaired feedback can alter IHC gene expression and maturation (Johnson et al., 2013). We conclude that $\alpha_2\delta3$ is not the main $\alpha_2\delta$ subunit of $Ca_v1.3$ channel complexes in IHCs, but may play a small role in their development.

$\alpha_2\delta3$ is clearly present in SG neurons (Fig. 4), the second level of auditory and acoustic SR processing (Fig. 1). Unfortunately, there are no reliable antibodies for unequivocally labeling the $\alpha_2\delta3$ protein. Nevertheless, the reduced somatic $Ca_v2.1$ protein level in $\alpha_2\delta3^{-/-}$ SG neurons reflects the role of $\alpha_2\delta3$ in membrane targeting of $Ca_v2.1$ subunits. The expression gradients of the somatic $Ca_v2.1$ protein in $\alpha_2\delta3^{+/+}$ (Fig. 6) and of the $\alpha_2\delta3$ reporter function (Fig. 4) along the tonotopic cochlear axis match tonotopic gradients described for other synaptic proteins in SG neurons, such as the GluR2/3 receptor (Flores-Otero and Davis, 2011).

Transmitter release in the CNS is mainly mediated by $Ca_v2.1$ and $Ca_v2.2$ channels (Catterall, 2000; Iwasaki et al., 2000). Mature cultured SG neurons express $Ca_v2.1$ currents at the soma and neurites (Lv et al., 2012). In slice recordings, $Ca_v2.1$ channels carry 85% of the presynaptic Ca^{2+} current at ANF endbulbs at P9–P11 (Lin et al., 2011) and are responsible for >80% of the evoked postsynaptic currents in VCN BCs at around P13 (Oleskevich and Walmsley, 2002). We postulate that the lack of $\alpha_2\delta3$ not only reduces $Ca_v2.1$ expression in the somata of SG neurons, but also in the synaptic terminals contacting BCs. The sparse $Ca_v2.1$ immunoreactivity at VGLUT1-positive ANF bou-

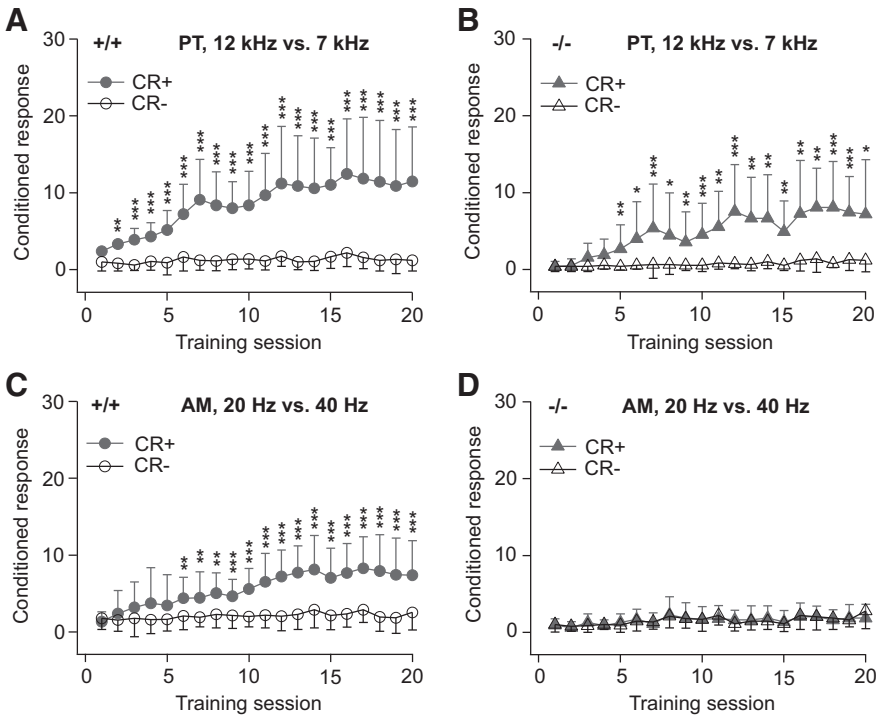

Figure 9. Discrimination learning of pure tones (PT) and temporally structured, amplitude-modulated (AM) tones. ***A–D***, The average numbers of hits (CR+) and false alarms (CR−) are plotted as a function of time (number of training session). For clarity, SD is plotted in one direction only (+SD for CR+, −SD for CR−). ***A***, ***B***, Learning curves of $\alpha_2\delta3^{+/+}$ (***A***, $n = 19$) and $\alpha_2\delta3^{-/-}$ (***B***, $n = 11$) mice for the PT discrimination task (12 kHz vs 7 kHz). ***C***, ***D***, Learning curves of $\alpha_2\delta3^{+/+}$ (***C***, $n = 20$) and $\alpha_2\delta3^{-/-}$ mice (***D***, $n = 12$) for the AM discrimination task (20 Hz-modulated pure tones vs 40 Hz-modulated pure tones; carrier frequency 12 kHz). $\alpha_2\delta3^{-/-}$ mice failed to learn to discriminate the two AM tones. Statistically significant differences between the CR+ and CR− rates were calculated for each training session, respectively. *$p < 0.05$ (Mann–Whitney U test). **$p < 0.01$ (Mann–Whitney U test). ***$p < 0.001$ (Mann–Whitney U test).

tons on BC somata in $\alpha_2\delta3^{+/+}$ mice (Fig. 7*A*) likely reflects the difficulty of labeling presynaptic VGCCs due to crowding and epitope masking at the active zone (Müller et al., 2010). Reduced numbers of presynaptic Ca^{2+} channels at $\alpha_2\delta3^{-/-}$ ANF synapses would result in less efficient synaptic transmission, with a reduced and delayed activation of BCs, as described for complexin I-deficient mice (Strenzke et al., 2009). Such a scenario matches the specific deviations of ABR waveforms in $\alpha_2\delta3^{-/-}$ mice, with reduced amplitude of wave II, which reflects auditory nerve transmission and relay to the CN (Henry and Lepkowski, 1978; Zhou et al., 2006). Juxtacellular recordings from sound-stimulated ANF–BC synapses showed reduced rate-level functions, reduced maximum spike rates, and increased first spike latencies in BC responses (Fig. 8), thus confirming defective synaptic transmission in $\alpha_2\delta3^{-/-}$.

Less efficient synaptic transmission and increased latencies at the endbulbs of Held may also explain the inability of $\alpha_2\delta3^{-/-}$ mice to discriminate temporally structured AM tones. Auditory neurons, from the cochlear nerve up to the auditory cortex, can fire phase-locked spikes in a precise way to each cycle of a temporally structured stimulus (e.g., to low modulation frequencies of AM tones) (Joris et al., 2004). Accurate temporal representations of sound can therefore be encoded across all relevant relay stations. An early ANF synaptic defect may thus cause an irreversible loss of the temporal information. Longer latencies (Fig. 8*E*) and the increased jitter, combined with a reduced number of spikes (i.e., loss of information) (Fig. 8*C*,*D*) in $\alpha_2\delta3^{-/-}$ neurons in sum, may lead to imprecise coding of AM tones. This results in significantly diminished information at those stations of the central auditory pathway that are involved in auditory discrimination learning and perception of AM tones, as demonstrated by our results on AM tone discrimination learning (Fig. 9*D*). The ability to discriminate pure tones, however, was not affected in $\alpha_2\delta3^{-/-}$ animals as they were able to use information in the spectral (not temporal) domain (Fig. 9*B*). This implies that $\alpha_2\delta3^{-/-}$ mice do not suffer from general auditory learning deficits. Because $\alpha_2\delta3$ is not only expressed in SG neurons, but also in auditory brainstem neurons (Fig. 4), imprecision in more central coding in the time domain may add to the ANF deficit. This may also explain the distorted ABR waves III and IV (Fig. 3*A*). Together, higher auditory centers will not be able to sufficiently extract precise information for perception and discrimination in the temporal domain.

The contribution of ANF synapses to the auditory and acoustic startle phenotype of $\alpha_2\delta3^{-/-}$ mice was strengthened by their altered morphology. Smaller ANF terminals in $\alpha_2\delta3^{-/-}$ mice can result in a diminished release capacity and impaired signaling in the auditory and acoustic startle pathway (Fig. 1). Smaller endbulbs of Held lacking intercellular cisterns have also been described in congenitally deaf Shaker-2 mice with nonfunctional mechano-electrical transduction (Lee et al., 2003). The endbulb phenotype of Shaker-2 mice most likely results from deprivation of auditory input due to cochlear deafness, whereas an auditory information stream is clearly present in $\alpha_2\delta3^{-/-}$ mice. Thus, altered endbulb morphology and reduced synaptic performance in $\alpha_2\delta3^{-/-}$ are likely caused by the local loss of $\alpha_2\delta3$ function, either directly (see below) or indirectly by reducing presynaptic Ca^{2+} channels. Synaptic malfunction, on the other hand, could also affect specific inhibitory pathways, thereby causing disinhibition, which might be responsible for the increased tactile SR (this study) or the cross-activation of cortical areas processing sensory information in $\alpha_2\delta3^{-/-}$ mice (Neely et al., 2010).

Our findings support the idea that $\alpha_2\delta3$ proteins are involved in synaptogenesis and maintenance of synapse structure (Dolphin, 2012). They are in line with results from *Drosophila*, where the $\alpha_2\delta3$ ortholog plays a crucial role in synaptogenesis and correct synapse morphology even independent of VGCC function (Dickman et al., 2008; Kurshan et al., 2009). In our study, we currently cannot distinguish between a direct and an indirect role of $\alpha_2\delta3$ (via regulating $Ca_v2.1$ channel expression) for proper ANF synapse formation. Morphological abnormalities of synapses were also found in Purkinje cells (Brodbeck et al., 2002) and at neuromuscular junctions of $\alpha_2\delta2$ mutant mice (Kaja et al., 2007). Recently, $\alpha_2\delta1$ was identified as the neural thrombospondin receptor responsible for synaptogenesis of central excitatory synapses, further pointing to a role of $\alpha_2\delta$ subunits in synaptic structuring (Eroglu et al., 2009).

Of interest, $\alpha_2\delta3$ appears to be a candidate in neuronal processing disorders. Neely et al. (2010) showed $\alpha_2\delta3$ being specifically required for thermal nociceptive signal transmission to

higher CNS areas. These results translate to humans, where polymorphisms in intronic sequence parts of CACNA2D3 are significantly associated with reduced heat pain sensitivity (Neely et al., 2010). Most recently, a splice site mutation in CACNA2D3 has been identified in children with autism spectrum disorders (Iossifov et al., 2012). Here we provide the first evidence of a multifunctional synaptic role of $\alpha_2\delta3$ that is essential for normal neuronal processing. Our findings propose a dual role of $\alpha_2\delta3$ for synaptic structure and function. As an auxiliary subunit, $\alpha_2\delta3$ promotes surface expression of $Ca_v2.1$ channel complexes in SG neurons and may modulate their gating properties, features controlling calcium microdomains and exocytosis. Second, $\alpha_2\delta3$ defines the morphology of ANF terminals, and its lack has profound consequences on synaptic transmission, leading to neuronal deficits in the auditory and the acoustic startle pathway. In conclusion, $\alpha_2\delta3^{-/-}$ mice provide a new and promising model to investigate sensory processing disorders in the context of calcium channelopathies.

References

Arikkath J, Campbell KP (2003) Auxiliary subunits: essential components of the voltage-gated calcium channel complex. Curr Opin Neurobiol 13:298–307. CrossRef Medline

Baig SM, Koschak A, Lieb A, Gebhart M, Dafinger C, Nürnberg G, Ali A, Ahmad I, Sinnegger-Brauns MJ, Brandt N, Engel J, Mangoni ME, Farooq M, Khan HU, Nurnberg P, Striessnig J, Bolz HJ (2011) Loss of Ca(v)1.3 (CACNA1D) function in a human channelopathy with bradycardia and congenital deafness. Nat Neurosci 14:77–84. CrossRef Medline

Barclay J, Balaguero N, Mione M, Ackerman SL, Letts VA, Brodbeck J, Canti C, Meir A, Page KM, Kusumi K, Perez-Reyes E, Lander ES, Frankel WN, Gardiner RM, Dolphin AC, Rees M (2001) Ducky mouse phenotype of epilepsy and ataxia is associated with mutations in the Cacna2d2 gene and decreased calcium channel current in cerebellar Purkinje cells. J Neurosci 21:6095–6104. Medline

Brandt A, Striessnig J, Moser T (2003) $Ca_V1.3$ channels are essential for development and presynaptic activity of cochlear inner hair cells. J Neurosci 23:10832–10840. Medline

Brodbeck J, Davies A, Courtney JM, Meir A, Balaguero N, Canti C, Moss FJ, Page KM, Pratt WS, Hunt SP, Barclay J, Rees M, Dolphin AC (2002) The ducky mutation in Cacna2d2 results in altered Purkinje cell morphology and is associated with the expression of a truncated α 2 δ-2 protein with abnormal function. J Biol Chem 277:7684–7693. CrossRef Medline

Catterall WA (2000) Structure and regulation of voltage-gated Ca^{2+} channels. Annu Rev Cell Dev Biol 16:521–555. CrossRef Medline

Cole RL, Lechner SM, Williams ME, Prodanovich P, Bleicher L, Varney MA, Gu G (2005) Differential distribution of voltage-gated calcium channel α-2 δ($\alpha2\delta$) subunit mRNA-containing cells in the rat central nervous system and the dorsal root ganglia. J Comp Neurol 491:246–269. CrossRef Medline

Davies A, Hendrich J, Van Minh AT, Wratten J, Douglas L, Dolphin AC (2007) Functional biology of the $\alpha(2)\delta$ subunits of voltage-gated calcium channels. Trends Pharmacol Sci 28:220–228. CrossRef Medline

Dickman DK, Kurshan PT, Schwarz TL (2008) Mutations in a Drosophila $\alpha2\delta$ voltage-gated calcium channel subunit reveal a crucial synaptic function. J Neurosci 28:31–38. CrossRef Medline

Dietz B, Jovanovic S, Wielsch B, Nerlich J, Rübsamen R, Milenkovic I (2012) Purinergic modulation of neuronal activity in developing auditory brainstem. J Neurosci 32:10699–10712. CrossRef Medline

Dolphin AC (2012) Calcium channel auxiliary $\alpha2\delta$ and beta subunits: trafficking and one step beyond. Nat Rev Neurosci 13:542–555. CrossRef Medline

Donato R, Page KM, Koch D, Nieto-Rostro M, Foucault I, Davies A, Wilkinson T, Rees M, Edwards FA, Dolphin AC (2006) The ducky(2J) mutation in Cacna2d2 results in reduced spontaneous Purkinje cell activity and altered gene expression. J Neurosci 26:12576–12586. CrossRef Medline

Engel J, Braig C, Rüttiger L, Kuhn S, Zimmermann U, Blin N, Sausbier M, Kalbacher H, Münkner S, Rohbock K, Ruth P, Winter H, Knipper M (2006) Two classes of outer hair cells along the tonotopic axis of the cochlea. Neuroscience 143:837–849. CrossRef Medline

Englitz B, Tolnai S, Typlt M, Jost J, Rübsamen R (2009) Reliability of synaptic transmission at the synapses of Held in vivo under acoustic stimulation. PloS One 4:e7014. CrossRef Medline

Eroglu C, Allen NJ, Susman MW, O'Rourke NA, Park CY, Ozkan E, Chakraborty C, Mulinyawe SB, Annis DS, Huberman AD, Green EM, Lawler J, Dolmetsch R, Garcia KC, Smith SJ, Luo ZD, Rosenthal A, Mosher DF, Barres BA (2009) Gabapentin receptor $\alpha2\delta$-1 is a neuronal thrombospondin receptor responsible for excitatory CNS synaptogenesis. Cell 139:380–392. CrossRef Medline

Flores-Otero J, Davis RL (2011) Synaptic proteins are tonotopically graded in postnatal and adult type I and type II spiral ganglion neurons. J Comp Neurol 519:1455–1475. CrossRef Medline

Fuller-Bicer GA, Varadi G, Koch SE, Ishii M, Bodi I, Kadeer N, Muth JN, Mikala G, Petrashevskaya NN, Jordan MA, Zhang SP, Qin N, Flores CM, Isaacsohn I, Varadi M, Mori Y, Jones WK, Schwartz A (2009) Targeted disruption of the voltage-dependent calcium channel $\alpha2/\delta$-1-subunit. Am J Physiol Heart Circ Physiol 297:H117–H124. CrossRef Medline

Glowatzki E, Fuchs PA (2000) Cholinergic synaptic inhibition of inner hair cells in the neonatal mammalian cochlea. Science 288:2366–2368. CrossRef Medline

Henry KR, Lepkowski CM (1978) Evoked potential correlates of genetic progressive hearing loss: age-related changes from the ear to the inferior colliculus of C57BL/6 and CBA/J mice. Acta Otolaryngol 86:366–374. CrossRef Medline

Hentschke M, Hentschke S, Borgmeyer U, Hübner CA, Kurth I (2009) The murine AE4 promoter predominantly drives type B intercalated cell specific transcription. Histochem Cell Biol 132:405–412. CrossRef Medline

Iossifov I, Ronemus M, Levy D, Wang Z, Hakker I, Rosenbaum J, Yamrom B, Lee YH, Narzisi G, Leotta A, Kendall J, Grabowska E, Ma B, Marks S, Rodgers L, Stepansky A, Troge J, Andrews P, Bekritsky M, Pradhan K, et al. (2012) De novo gene disruptions in children on the autistic spectrum. Neuron 74:285–299. CrossRef Medline

Iwasaki S, Momiyama A, Uchitel OD, Takahashi T (2000) Developmental changes in calcium channel types mediating central synaptic transmission. J Neurosci 20:59–65. Medline

Johnson SL, Kuhn S, Franz C, Ingham N, Furness DN, Knipper M, Steel KP, Adelman JP, Holley MC, Marcotti W (2013) Presynaptic maturation in auditory hair cells requires a critical period of sensory-independent spiking activity. Proc Natl Acad Sci U S A 110:8720–8725. CrossRef Medline

Joris PX, Schreiner CE, Rees A (2004) Neural processing of amplitude-modulated sounds. Physiol Rev 84:541–577. CrossRef Medline

Kaja S, Todorov B, van de Ven RC, Ferrari MD, Frants RR, van den Maagdenberg AM, Plomp JJ (2007) Redundancy of Cav2.1 channel accessory subunits in transmitter release at the mouse neuromuscular junction. Brain Res 1143:92–101. CrossRef Medline

Knirsch M, Brandt N, Braig C, Kuhn S, Hirt B, Münkner S, Knipper M, Engel J (2007) Persistence of $Ca_v1.3$ Ca^{2+} channels in mature outer hair cells supports outer hair cell afferent signaling. J Neurosci 27:6442–6451. CrossRef Medline

Kurshan PT, Oztan A, Schwarz TL (2009) Presynaptic $\alpha2\delta$-3 is required for synaptic morphogenesis independent of its Ca^{2+}-channel functions. Nat Neurosci 12:1415–1423. CrossRef Medline

Kurt S, Ehret G (2010) Auditory discrimination learning and knowledge transfer in mice depends on task difficulty. Proc Natl Acad Sci U S A 107:8481–8485. CrossRef Medline

Kurt S, Fisher SE, Ehret G (2012a) Foxp2 mutations impair auditory-motor association learning. PloS One 7:e33130. CrossRef Medline

Kurt S, Sausbier M, Rüttiger L, Brandt N, Moeller CK, Kindler J, Sausbier U, Zimmermann U, van Straaten H, Neuhuber W, Engel J, Knipper M, Ruth P, Schulze H (2012b) Critical role for cochlear hair cell BK channels for coding the temporal structure and dynamic range of auditory information for central auditory processing. FASEB J 26:3834–3843. CrossRef Medline

Lappe-Siefke C, Loebrich S, Hevers W, Waidmann OB, Schweizer M, Fehr S, Fritschy JM, Dikic I, Eilers J, Wilson SM, Kneussel M (2009) The ataxia (axJ) mutation causes abnormal GABAA receptor turnover in mice. PLoS Genet 5:e1000631. CrossRef Medline

Lee DJ, Cahill HB, Ryugo DK (2003) Effects of congenital deafness in the cochlear nuclei of Shaker-2 mice: an ultrastructural analysis of synapse morphology in the endbulbs of Held. J Neurocytol 32:229–243. CrossRef Medline

Lin KH, Oleskevich S, Taschenberger H (2011) Presynaptic Ca^{2+} influx and

vesicle exocytosis at the mouse endbulb of Held: a comparison of two auditory nerve terminals. J Physiol 589:4301–4320. CrossRef Medline

Lv P, Sihn CR, Wang W, Shen H, Kim HJ, Rocha-Sanchez SM, Yamoah EN (2012) Posthearing Ca^{2+} currents and their roles in shaping the different modes of firing of spiral ganglion neurons. J Neurosci 32:16314–16330. CrossRef Medline

Müller CS, Haupt A, Bildl W, Schindler J, Knaus HG, Meissner M, Rammner B, Striessnig J, Flockerzi V, Fakler B, Schulte U (2010) Quantitative proteomics of the Ca_v2 channel nano-environments in the mammalian brain. Proc Natl Acad Sci U S A 107:14950–14957. CrossRef Medline

Neef J, Gehrt A, Bulankina AV, Meyer AC, Riedel D, Gregg RG, Strenzke N, Moser T (2009) The Ca^{2+} channel subunit beta2 regulates Ca^{2+} channel abundance and function in inner hair cells and is required for hearing. J Neurosci 29:10730–10740. CrossRef Medline

Neely GG, Hess A, Costigan M, Keene AC, Goulas S, Langeslag M, Griffin RS, Belfer I, Dai F, Smith SB, Diatchenko L, Gupta V, Xia CP, Amann S, Kreitz S, Heindl-Erdmann C, Wolz S, Ly CV, Arora S, Sarangi R, et al. (2010) A genome-wide Drosophila screen for heat nociception identifies $\alpha2\delta3$ as an evolutionarily conserved pain gene. Cell 143:628–638. CrossRef Medline

Oleskevich S, Walmsley B (2002) Synaptic transmission in the auditory brainstem of normal and congenitally deaf mice. J Physiol 540:447–455. CrossRef Medline

Pilz PK, Schnitzler HU (1996) Habituation and sensitization of the acoustic startle response in rats: amplitude, threshold, and latency measures. Neurobiol Learn Mem 66:67–79. CrossRef Medline

Pilz PK, Carl TD, Plappert CF (2004) Habituation of the acoustic and the tactile startle responses in mice: two independent sensory processes. Behav Neurosci 118:975–983. CrossRef Medline

Plappert CF, Kuhn S, Schnitzler HU, Pilz PK (2006) Experience increases the prepulse inhibition of the acoustic startle response in mice. Behav Neurosci 120:16–23. CrossRef Medline

Platzer J, Engel J, Schrott-Fischer A, Stephan K, Bova S, Chen H, Zheng H, Striessnig J (2000) Congenital deafness and sinoatrial node dysfunction in mice lacking class D L-type Ca^{2+} channels. Cell 102:89–97. CrossRef Medline

Rüttiger L, Singer W, Panford-Walsh R, Matsumoto M, Lee SC, Zuccotti A, Zimmermann U, Jaumann M, Rohbock K, Xiong H, Knipper M (2013) The reduced cochlear output and the failure to adapt the central auditory response causes tinnitus in noise exposed rats. PloS One 8:e57247. CrossRef Medline

Schindelin J, Arganda-Carreras I, Frise E, Kaynig V, Longair M, Pietzsch T, Preibisch S, Rueden C, Saalfeld S, Schmid B, Tinevez JY, White DJ, Hartenstein V, Eliceiri K, Tomancak P, Cardona A (2012) Fiji: an open-source platform for biological-image analysis. Nat Methods 9:676–682. CrossRef Medline

Simmons DD (2002) Development of the inner ear efferent system across vertebrate species. J Neurobiol 53:228–250. CrossRef Medline

Simons-Weidenmaier NS, Weber M, Plappert CF, Pilz PK, Schmid S (2006) Synaptic depression and short-term habituation are located in the sensory part of the mammalian startle pathway. BMC Neurosci 7:38. CrossRef Medline

Singer W, Panford-Walsh R, Watermann D, Hendrich O, Zimmermann U, Köpschall I, Rohbock K, Knipper M (2008) Salicylate alters the expression of calcium response transcription factor 1 in the cochlea: implications for brain-derived neurotrophic factor transcriptional regulation. Mol Pharmacol 73:1085–1091. CrossRef Medline

Strenzke N, Chanda S, Kopp-Scheinpflug C, Khimich D, Reim K, Bulankina AV, Neef A, Wolf F, Brose N, Xu-Friedman MA, Moser T (2009) Complexin-I is required for high-fidelity transmission at the endbulb of held auditory synapse. J Neurosci 29:7991–8004. CrossRef Medline

Typlt M, Haustein MD, Dietz B, Steinert JR, Witte M, Englitz B, Milenkovic I, Kopp-Scheinpflug C, Forsythe ID, Rübsamen R (2010) Presynaptic and postsynaptic origin of multicomponent extracellular waveforms at the endbulb of Held-spherical bushy cell synapse. Eur J Neurosci 31:1574–1581. CrossRef Medline

Winter H, Rüttiger L, Müller M, Kuhn S, Brandt N, Zimmermann U, Hirt B, Bress A, Sausbier M, Conscience A, Flamant F, Tian Y, Zuo J, Pfister M, Ruth P, Löwenheim H, Samarut J, Engel J, Knipper M (2009) Deafness in TRbeta mutants is caused by malformation of the tectorial membrane. J Neurosci 29:2581–2587. CrossRef Medline

Zampini V, Johnson SL, Franz C, Lawrence ND, Münkner S, Engel J, Knipper M, Magistretti J, Masetto S, Marcotti W (2010) Elementary properties of $Ca_V1.3$ $Ca(2+)$ channels expressed in mouse cochlear inner hair cells. J Physiol 588:187–199. CrossRef Medline

Zhou X, Jen PH, Seburn KL, Frankel WN, Zheng QY (2006) Auditory brainstem responses in 10 inbred strains of mice. Brain Res 1091:16–26. CrossRef Medline